Impact of the growth temperature on the performance of 1.70-eV $Al_{0.22}Ga_{0.78}As$ solar cells grown by MBE

Arthur Onno[1]*, Mingchu Tang[1], Lars Oberbeck[2], Jiang Wu[1], Huiyun Liu[1]

[1]Department of Electronic and Electrical Engineering, University College London, London WC1E 7JE, United Kingdom

[2]TOTAL Gas, Renewables & Power, 92069 Paris La Défense, France

ABSTRACT

Growth of high material quality Aluminum Gallium Arsenide ($Al_xGa_{1-x}As$) is known to be challenging, in particular with an Al content *x* above 20%. As a result, the use of $Al_xGa_{1-x}As$ in devices requiring high minority carrier lifetimes, such as solar cells, has been limited. Nonetheless, it has long been established that the substrate temperature is a key parameter in improving $Al_xGa_{1-x}As$ material quality. In order to optimize the growth temperature of 1.70-eV $Al_{0.22}Ga_{0.78}As$ solar cells, five samples have been grown by Solid-Source Molecular Beam Epitaxy (SSMBE) at 580°C, 600°C, 620°C, 640°C, and 660°C, respectively. A strong improvement in performance is observed with increasing the growth temperature from 580°C to 620°C. An open-circuit voltage above 1.21V has in particular been demonstrated on the sample grown at 620°C, translating into a bandgap-voltage offset W_{oc} below 0.5V. Above 620°C, performances – in particular the short-circuit current density – moderately decrease. This trend is confirmed by photoluminescence, current density versus voltage characterization under illumination, and external quantum efficiency measurements.

Keywords
B2. Aluminum Gallium Arsenide; B3. Solar Cells; A3. Molecular Beam Epitaxy; A3. Growth Temperature

Corresponding author

Arthur Onno, Department of Electronic and Electrical Engineering, University College London, London WC1E 7JE, United Kingdom

E-mail: arthur.onno.13@ucl.ac.uk

1. INTRODUCTION

The ternary III-V compound Aluminum Gallium Arsenide ($Al_xGa_{1-x}As$), with a tunable direct bandgap ranging from 1.42eV (pure GaAs at x=0) to about 2.0eV (Γ-valley/X-Valley transition at x=0.45) [1-2] and a lattice parameter closely matching the one of commercially available GaAs substrates [1], has been widely studied for optoelectronic applications. It is commonly epitaxially grown by Molecular Beam Epitaxy (MBE) and Metal-Organic Chemical Vapor Deposition (MOCVD).

The main challenge regarding the epitaxial growth of $Al_xGa_{1-x}As$ lies in the substantial incorporation of contaminants – in particular oxygen [3] – during deposition, leading to a high density of deep level defects related to Al-O complexes [4-5], and subsequently to a reduced minority carrier diffusion length [6] and lifetime [7]. This issue has been reported for materials grown using MBE and MOCVD systems [4-7]. As a result, the use of $Al_xGa_{1-x}As$ in applications strongly dependent on long minority carrier lifetimes, such as photovoltaic solar cells, has been limited.

Extensive studies have been carried out in the past on high aluminum content ($x \geq 20\%$) $Al_xGa_{1-x}As$ solar cells grown by MBE [6,8-11] and MOCVD [12-15]. Most of these early devices exhibit poor performances, in particular a low open-circuit voltage (V_{oc}) in regard of the bandgap of the active material. Consequently, although III-V based multijunction solar cells are commercially available for space and concentrator applications, none of these high efficiency devices currently integrates an $Al_xGa_{1-x}As$ subcell; and $In_{0.49}Ga_{0.51}P$ is now the material of choice for high bandgap (1.9eV) subcells.

$Al_xGa_{1-x}As$ photovoltaic solar cells have recently experienced a renewal of interest [16-17], due in part to the need of subcells with a bandgap between 1.4 and 1.9eV for multijunction solar cells using four or more junctions [18]. Additionally, high efficiency 1.9-eV $Al_{0.37}Ga_{0.63}As$ could replace $In_{0.49}Ga_{0.51}P$ in current 3-junction multijunction solar cells, avoiding the high cost associated with the use of indium [17]. Finally, following the recent progress in the development of a low threading dislocation density platform to monolithically integrate high material quality GaAs and $Al_xGa_{1-x}As$ on Si [19-20], 1.70-eV $Al_{0.22}Ga_{0.78}As$ presents a strong interest as a top cell absorber material in tandem dual-junction III-V/Si photovoltaic applications. Such low threading dislocation density 1.70-eV $Al_{0.22}Ga_{0.78}As$ solar cells have been recently grown by MBE on Si substrates [21-22]. However, these initial devices, all grown at a substrate temperature of 580°C, have shown poor performances – in particular low V_{oc} values under 1150mV – even for the reference cells grown lattice-matched on GaAs.

Growth temperature has long been established as a key parameter in order to reduce oxygen contamination, and thus to enhance the material quality and performance of $Al_xGa_{1-x}As$ solar cells [6,8-9,11], with the optimal temperature greatly dependent on the Al content x. In this contribution, we present and discuss recent progress in the MBE growth of 1.70-eV $Al_{0.22}Ga_{0.78}As$ solar cells on GaAs substrates. The growth temperature in particular has been optimized: five samples have been grown at 580°C, 600°C, 620°C, 640°C, and 660°C, respectively. A clear improvement is demonstrated with increasing the growth temperature from 580-600°C to 620°C. Above 620°C, the performance of the cells declines moderately. At 660°C, the Al to Ga ratio in the cell starts to be impacted, with a lower Ga incorporation, and the bandgap of the cell is increased above the desired 1.70eV value.

2. EXPERIMENTAL METHOD

2.1. Samples growth

The five samples were grown in a Veeco GEN930 Solid-Source Molecular Beam Epitaxy (SSMBE). Growth temperatures were monitored using a thermocouple mounted on the back of the wafer holder and an external infrared pyrometer. All the growth temperatures reported hereafter correspond to estimate real temperatures, extrapolated from the thermocouple readings. The well-documented transition of the Reflection High Energy Electron Diffraction (RHEED) pattern at 580°C [23] – characteristic of the in-situ thermal desorption of the native oxide present on the substrate prior to growth – was used to calibrate this linear extrapolation. The epilayers were doped using Si (n-type regions) and Be (p-type regions) solid sources. All growth runs have been performed on standard n-type GaAs (100) substrates.

The structure of the cells is presented in FIGURE 1. After in-situ desorption of the native oxide layer present on the surface of the substrate, controlled through RHEED, a 200nm-thick n^+-GaAs ($N_d=1.4\times10^{18}cm^{-3}$) buffer is grown, followed by a 1µm-thick n^+-$Al_{0.22}Ga_{0.78}As$ ($N_d=1.1\times10^{18}cm^{-3}$) contacting layer, in order to allow eventual contacting from the top after mesa etching. The cell itself consists of a 2µm-thick n-type $Al_{0.22}Ga_{0.78}As$ base ($N_d=2\times10^{17}cm^{-3}$), a 120nm-thick p^+-type $Al_{0.22}Ga_{0.78}As$ ($N_a=1\times10^{18}cm^{-3}$) emitter, and a 50nm-thick p^+-AlAs/$Al_{0.5}Ga_{0.5}As$ ($N_a=4\times10^{18}cm^{-3}$) superlattice window layer. The cell is capped by a highly doped 50nm-thick p^+-GaAs ($N_a=1\times10^{19}cm^{-3}$) contacting layer. This contacting layer also protects the underlying AlAs/$Al_{0.5}Ga_{0.5}As$ superlattice from oxidation. The structure grown does not include a Back Surface Field (BSF).

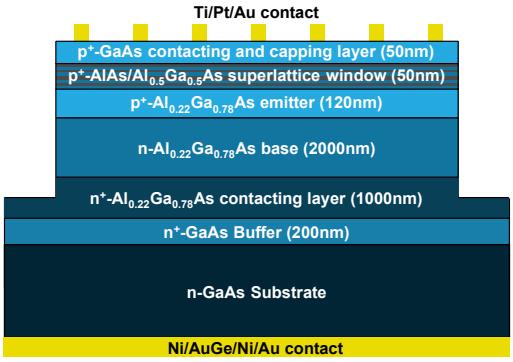

Figure 1. Structure of the samples, grown and processed into devices.

2.2. Device fabrication

Following growth, contact to the n-type region was thermally evaporated on the full back surface of the samples. A Ni/AuGe/Ni/Au (5nm/100nm/30nm/200nm) contact structure was deposited and subsequently annealed at 390°C for 60s. Individual devices' front grids were defined by standard photolithography techniques before sputtering of the Ti/Pt/Au (20nm/50nm/400nm) contact to the p-type region. After contact lift-off, another photolithography step was performed to delimit the surface of the devices. Wet mesa etching was then carried out using a H_2SO_4:H_2O_2:H_2O (1:10:80) selective etching solution, thus electrically isolating 5mm×5mm and 3mm×3mm square devices. No anti-reflection coating was deposited. Moreover, in

order to protect the underlying AlAs/$Al_{0.5}Ga_{0.5}As$ superlattice window, the top GaAs capping and contacting layer was not etched around the contacts. This leads to a non-negligible parasitic absorption in the lower bandgap (1.42eV) 50nm-thick GaAs contacting layer. Using a classic Beer-Lambert absorption model, the associated short-circuit current density (J_{sc}) loss has been evaluated at around 5.5mA.cm^{-2} to 6mA.cm^{-2}, in addition to reflection losses.

2.3. Characterization

Structural properties of the samples have been investigated using Atomic Force Microscopy (AFM) and X-Ray Diffraction (XRD). AFM imaging has been carried out at room-temperature in a Veeco Nanoscope Dimension V 3100 SPM system, in tapping mode. A Jordan Valley D1 instrument has been used for XRD measurements. Given the narrow difference in lattice parameters between GaAs and $Al_xGa_{1-x}As$, we assume no relaxation of the epilayers. The Al content x of the samples can thus be extracted from the XRD ω-2θ graphe, by analyzing the difference between the substrate intensity peak and the epilayers intensity peak.

Steady-state room-temperature photoluminescence (PL) emission spectra of the grown samples were acquired in a Nanometrics RPM2000 rapid photoluminescence mapping system, allowing direct comparison between the samples.

Current density versus voltage (J-V) characteristics under illumination, illumination intensity versus open-circuit voltage (Suns-V_{oc}) measurements and External Quantum Efficiency (EQE) measurements were acquired in order to analyze the photovoltaic and diode properties of the fabricated devices.

J-V characteristics were acquired using a Keithley 2400 sourcemeter coupled with ReRa Tracer 3.0 software. A LOT solar simulator, fitted with a filtered xenon lamp calibrated to reproduce the AM1.5G spectrum at 100mW.cm^{-2}, was used for measurements under illumination. As the front grid contact to the p-type region covers a non-negligible portion of the fabricated devices (4.29mm^2 for the 5×5mm devices, 1.93mm^2 for the 3×3mm devices), the current density results presented hereafter correspond to the designated area of the devices (20.71mm^2 for the 5×5mm devices, 7.07mm^2 for the 3×3mm devices) in order to allow meaningful comparison between devices of different size.

Suns-V_{oc} measurements were performed in a Sinton Instruments system. In order to rectify the strong spectral mismatch between the 1.70-eV $Al_{0.22}Ga_{0.78}As$ measured cell and the 1.12-eV Si cell used to determine the illumination intensity [24], a Schott KG3 short pass filter was placed in front of the illumination intensity monitoring cell. This reduced the difference in measured V_{oc} at 1 sun between the J-V setup and the Suns-V_{oc} system to 5 to 10 mV, depending on the spectral response of the sample. An additional spectral mismatch coefficient was consequently calculated for each device to match the J-V and Suns-V_{oc} measurements [24].

Room-temperature EQE measurements were performed with a SpeQuest Quantum efficiency system from ReRa.

2.4. Results analysis

The bandgap of the grown material can vary from one sample to another, and even from device to device on the same wafer for high temperature growth runs. As a result, the V_{oc} of an individual cell, directly dependent on the bandgap, can be a

misleading parameter to evaluate the material quality of the device. The bandgap-voltage offset W_{oc}, defined as:

$$W_{oc} = \frac{E_g}{q} - V_{oc} \tag{1}$$

presents the advantage of allowing comparison between samples with different bandgaps. As a result, a precise evaluation of the bandgap is needed. As presented in ref. [25], for direct bandgap materials, the difference between the photons energy E_{ph} and the bandgap E_g verifies:

$$\left[E_{ph} \times \ln(1 - EQE)\right]^2 \propto E_{ph} - E_g \tag{2}$$

The bandgap can be precisely calculated for each device, based on the device EQE, by linearly fitting the left part of Equation (2) and finding the intersection of this linear fit with the horizontal axis.

3. RESULTS AND DISCUSSION

3.1. Structural characterization

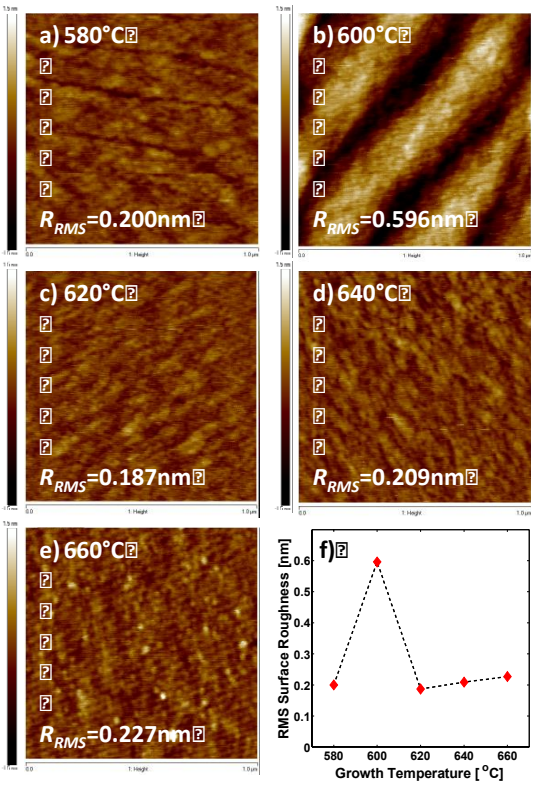

Figure 2. Atomic Force Microscopy imaging of the samples grown at 580°C (a), 600°C (b), 620°C (c), 640°C (d) and 660°C (e). All images show a 1×1µm surface with identical -1.5nm to +1.5nm color bar scales. The root mean squared surface roughness as a function of the growth temperature is also displayed (f).

AFM images of the five samples grown are displayed in FIGURE 2a-2e, each image representing a surface of 1µm×1µm with a -1.5nm to +1.5nm scale. The root mean

squared surface roughness R_{RMS} is also displayed as a function of the growth temperature (FIGURE 2f). All samples, except from the one grown at 600°C, exhibit very smooth surfaces with R_{RMS} in the order of magnitude of 0.2nm. On the other hand, the sample grown at 600°C exhibits a poor surface morphology, with an R_{RMS} close to 0.6nm. AFM characterization of additional samples grown at 600°C, 620°C, and 640°C with an undoped emitter gave comparable results: the additional samples grown at 620°C and 640°C exhibit smooth surfaces with an R_{RMS} around 0.2nm, while the sample grown at 600°C presents a poor surface morphology, with a similar directional streaky pattern and an R_{RMS} around 0.6nm. The surface roughness for the growth at 600°C is thus reproducible. The existence of a "forbidden temperature window" for the growth of high Al content (x>20%) $Al_xGa_{1-x}As$ – with samples grown in that temperature window exhibiting a poor surface morphology – has been widely reported [26-27]. Although the exact mechanism responsible for this so-called "forbidden window" is still unclear, the authors believe that, in the present case, the poor surface morphology of the samples grown at 600°C is an occurrence of such a "forbidden temperature window".

The Al content of the samples, extracted from XRD, are compiled in TABLE 1, as well as the corresponding difference between the substrate and epilayers intensity peaks in the ω-2θ graph. The samples grown at or under 640°C exhibit Al contents close to the 22% expected from the Ga/Al flux ratio calibrated through RHEED intensity fluctuation, assuming a sticking coefficient equal to one for both atomic species. The sample grown at 660°C, however, presents a higher Al content of 28.0%. This is caused by the re-evaporation of Ga from the growth surface above 650°C [28], leading to a Ga incorporation below unity while Al adatoms are still fully incorporated. As a result, a higher bandgap is expected for the sample grown at 660°C.

T [°C]	R_{RMS} [nm]	ω-2θ [arcsec]	Al content [%]
580	0.200	79	21.7
600	0.596	80	21.9
620	0.187	80	21.9
640	0.209	80	21.9
660	0.227	102	28.0

Table 1. Root mean squared surface roughness R_{RMS} – calculated from AFM – and Al content x – extracted from XRD – of the samples grown at different temperatures T. The ω-2θ difference between the XRD intensity peaks of the GaAs substrate and the $Al_xGa_{1-x}As$ epilayers is also reported.

3.2. Photoluminescence

A PL comparison of the samples is displayed in FIGURE 3. The PL measurements are taken from the center of the wafers, where the temperature is measured by the thermocouple during growth. The four samples grown at 580°C (magenta diamonds), 600°C (black crosses), 620°C (red asterisks) and 640°C (blue squares) exhibit a peak

intensity wavelength between 726.6nm and 728.7nm, corresponding to the 1.70-eV bandgap expected from $Al_{0.22}Ga_{0.78}As$, in agreement with the Al content extracted from XRD. On the other hand, for the sample grown at 660°C (green circles), the PL signal peaks at 701nm, corresponding to a bandgap of 1.77eV, again in agreement with the Al content of x=28% calculated from XRD.

It is to be noted that, in contrast with the other samples, the wafer grown at 660°C presents a gradient of peak intensity wavelengths across its surface: from 700nm in the center of the wafer to 727nm on its edge. This unusual PL distribution originates from the use of a single-filament substrate heater, leading to a temperature gradient across the wafer, with a higher temperature in the center of the wafer and a lower temperature on the edge, where thermal losses are stronger due to geometry. Although the growth temperature in the center of the wafer (660°C) is above the re-evaporation temperature of Ga (650°C) [28], leading to a limited Ga incorporation, the temperature on the edges is likely under this threshold and the sticking coefficient of Ga is close to 1. Consequently, the PL peak wavelength on the edge of the wafer is closer to the 729nm expected from a 1.70-eV bandgap material.

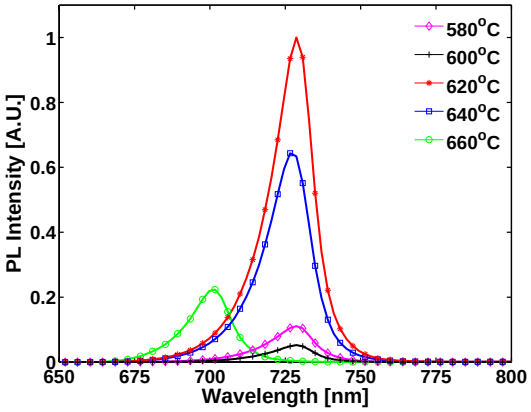

Figure 3. Photoluminescence (PL) comparison of the samples grown at 580°C (magenta diamonds), 600°C (black crosses), 620°C (red asterisks), 640°C (blue squares) and 660°C (green circles). The higher material quality with a growth temperature of 620°C is apparent, as well as the higher bandgap due to the lower Ga incorporation with a growth temperature of 660°C, resulting in a strong blue shift of the PL peak intensity.

Comparatively low peak intensities have been measured for the samples grown at 580°C and 600°C, with the sample grown at 600°C exhibiting a lesser signal. This is in agreement with the poor surface morphology of that sample, observed by AFM. The strongest PL peak intensity is obtained at 620°C and decreases at higher growth temperatures, indicating a superior $Al_{0.22}Ga_{0.78}As$ material quality at a growth temperature of 620°C. This is in accordance with the lower surface roughness measured by AFM.

3.3. Photovoltaic properties

The Current density versus Voltage (J-V) characteristics, acquired under illumination, of the highest efficiency devices fabricated on each sample are displayed in FIGURE 4 (solid lines). No evident difference has been observed between the 3×3mm and the 5×5mm devices. Hereafter, they are consequently reported in an undifferentiated

manner. The pseudo J-V characteristics, extracted from Suns-V_{oc} measurements, are also displayed (dashed lines). The main parameters of these best-performing cells are reported in TABLE 2. As expected from PL and AFM studies, the sample grown at 620°C (red lines with asterisks) exhibits the best performances, in terms of short-circuit current density (J_{sc}) as well as in terms of open-circuit voltage (V_{oc}) and efficiency. Moreover, a strong improvement in performance is achieved by increasing the growth temperature from 580-600°C to 620°C. The sample grown at 600°C, presenting a poor surface morphology, exhibit a particularly low V_{oc}. Above 620°C the performance moderately decrease, in particular due to a reduction of J_{sc}.

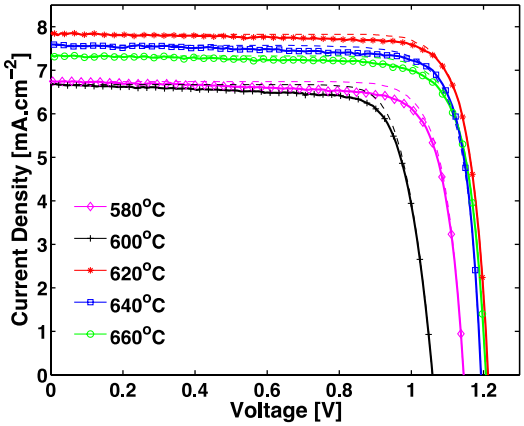

Figure 4. Current density versus Voltage (J-V) characterizations (solid lines), acquired under illumination, and pseudo J-V characterizations (dashed lines), extracted from Suns-V_{oc} measurements, of the highest efficiency device fabricated from each sample grown.

T [°C]	V_{oc} [mV]	J_{sc} [mA.cm^{-2}]	FF [%]	Efficiency [%]	Pseudo FF [%]	Pseudo Efficiency [%]
580	1145	6.75	79.3	6.12	82.0	6.34
600	1058	6.68	78.0	5.52	81.0	5.72
620	1212	7.85	81.7	7.77	82.4	7.84
640	1194	7.58	81.8	7.39	81.5	7.37
660	1207	7.34	80.5	7.12	81.9	7.25

Table 2. Main parameters of the highest efficiency devices fabricated from each sample. The open-circuit voltages (V_{oc}), short-circuit-currents (J_{sc}), Fill Factors (FF) and efficiencies have been extracted from the J-V curves presented in FIGURE 4. The pseudo FF and pseudo efficiencies have been extracted from the corresponding pseudo J-V curves, also in FIGURE 4.

For each sample, 22 to 44 devices have been fabricated, depending on the size and the geometry of the portion of wafer processed. In order to better assess the trends at play and to eliminate possible inconsistencies arising from inhomogeneities during growth or fabrication, the main metrics of the highest efficiency device (red diamonds) and, for each of these considered metrics, of the 25% best performing cells (black cross

and dashed line = average value, whiskers = distribution) for each sample are displayed in FIGURE 5. The open-circuit voltages V_{oc} (a), bandgap-voltage offsets W_{oc} (b), short-circuit currents J_{sc} (c) and efficiencies (d) are reported.

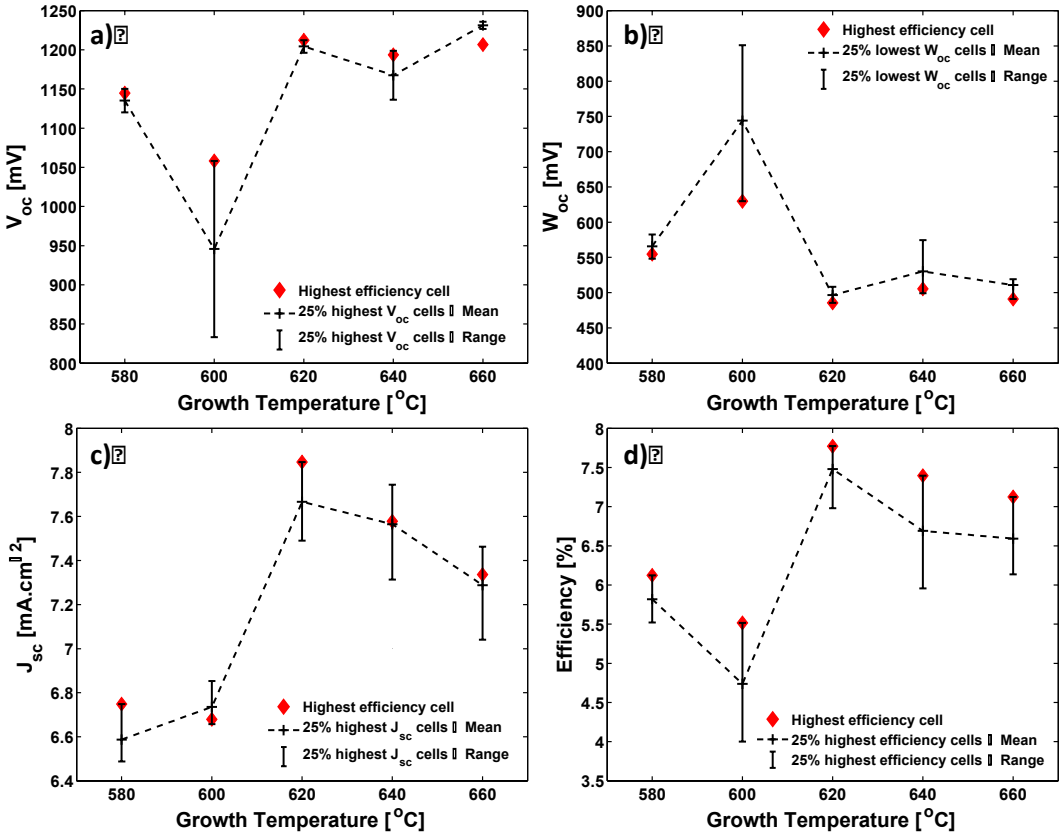

Figure 5. Comparison of the open-circuit voltage V_{oc} (a), bandgap-voltage offset W_{oc} (b), short-circuit current J_{sc} (c) and efficiency (d) of the highest efficiency device fabricated on each sample (red diamonds) and of the 25% best performing devices for the given metric (black cross and dashed lines = mean value, whiskers = range).

In agreement with sections 3.1 and 3.2, the sample grown at 600°C presents poor V_{oc}, W_{oc}, and efficiency for the best device, as well as a wide distribution of these metrics across the best performing devices. The J_{sc} is however weakly impacted, with a distribution of highest J_{sc} values similar to the other samples. The distribution of bandgap across the sample grown at 660°C is also apparent, with this sample exhibiting the highest V_{oc} values, although the W_{oc} values are similar to the ones obtained at 620-640°C. In particular, the highest efficiency device reported in FIGURE 4, fabricated from the extreme edge of the wafer – where the Al content and thus the bandgap is lower – is not amongst the 25% highest V_{oc} values measured across the wafer, as higher bandgap devices from the center of the wafer achieve higher V_{oc} values.

As expected from AFM and PL measurements, the sample grown at 620°C presents the best performance in terms of J_{sc}, W_{oc} and efficiency. The measured V_{oc} (1212mV) is close to the record value of 1.22V reported for 1.70-eV $Al_{0.22}Ga_{0.78}As$ solar cells grown by MBE [10]. This is especially significant given the comparatively low J_{sc} achieved in this study; due to parasitic absorption in the GaAs top capping and

contacting layer (not-etched) and the lack of an anti-reflection coating. Assuming a doubling of the J_{sc} with an improved fabrication process, including etching of the GaAs capping layer and deposition of an anti-reflection coating, an expected V_{oc} of 1241mV has been calculated from the Suns-V_{oc} measurements, as a result of the improved quasi-Fermi levels separation due to stronger light absorption.

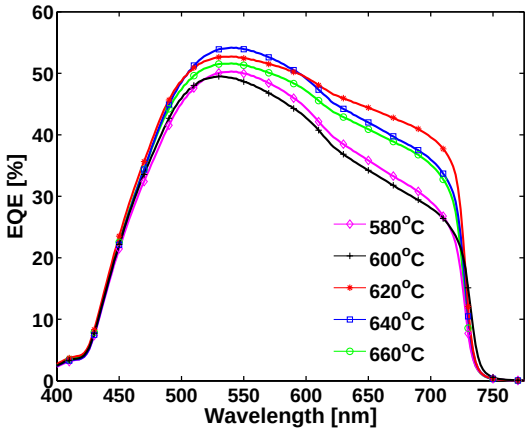

Figure 6. External Quantum Efficiency (EQE) of the highest efficiency device fabricated from each grown sample.

The trend in material quality is particularly apparent from the analysis of the J_{sc} values (FIGURE 5c), with a strong improvement from 580-600°C to 620°C and a moderate decrease above 620°C. Notwithstanding the sample grown at 600°C, this trend is confirmed by the analysis of the efficiencies of the best devices.

EQE measurements of the highest efficiency device from each sample are reported in FIGURE 6. Absolute EQEs have been calculated based on the J_{sc} measured during J-V characterization under AM1.5G illumination. The improvement in material quality when increasing the growth temperature from 580°C to 620°C is apparent, with an enhancement of the quantum efficiency – especially for lower energy photons – indicating an increase in minority carrier diffusion length. Above 620°C, the quantum efficiency is reduced at longer wavelengths as the material quality and thus the minority carrier diffusion length decrease. The stronger response around 550nm for the sample grown at 640°C is of unknown origin and further characterization is needed to fully understand the phenomenon at play.

The lower EQE at longer wavelengths, with a characteristic shoulder in the EQE curve close to the band-edge, is a well-known phenomenon for $Al_xGa_{1-x}As$ solar cells [8-12]. It has been demonstrated that this issue can be addressed by using Se instead of Si as the dopant for the n-type regions [15].

4. CONCLUSION

In order to optimize $Al_{0.22}Ga_{0.78}As$ material quality, 1.70-eV $Al_{0.22}Ga_{0.78}As$ photovoltaic solar cells have been grown by Molecular Beam Epitaxy (MBE) at 580°C, 600°C, 620°C, 640°C, and 660°C. Analyses of the surface roughnesses and photoluminescence (PL) peak intensities show an improvement in material quality with increasing the growth temperature from 580°C to 620°C. Notably, the sample grown at 600°C presents a poor surface morphology, leading to limited optoelectronic

performance. The best material properties are achieved at 620°C, with both surface roughness and PL peak intensity gradually degrading when increasing the growth temperature above 620°C.

In contrast with the samples grown at lower temperatures, a greater Al content of 28.0% is obtained when the growth temperature is increased to 660°C, as demonstrated by X-Ray Diffraction (XRD) measurements. This is due to Ga re-evaporation from the growth surface above 650°C, leading to a Ga sticking coefficient below unity while Al incorporation is not impacted. As a result, the Ga to Al ratio is reduced and the Al content is increased. The bandgap of the sample is thus widened, as confirmed from PL measurements.

Optoelectronic characterization of the devices fabricated from the five grown samples confirms the trend outlined by the surface roughness and PL analyses, with a clear improvement of photovoltaic properties when increasing the growth temperature from 580-600°C to 620°C, and a moderate decrease beyond 620°C. The trend is particularly apparent when analyzing the highest short-circuit currents (J_{sc}) measured across each sample: contrary to the open-circuit voltage (V_{oc}) and bandgap-voltage offset (W_{oc}) – which can suffer from an eventual contamination at the p-n interface – the J_{sc} is directly linked to the minority carrier diffusion length, and hence the lifetime, throughout the epilayers. In case of a potential contamination specific to the depletion region, the J_{sc} is therefore a good metric to assess the bulk material quality.

Overall, the sample grown at 620°C exhibits the best material properties and photovoltaic performance, with the lowest W_{oc} and the highest J_{sc} and efficiency measured. An open-circuit voltage of 1212mV has been demonstrated, corresponding to a W_{oc} below 500mV. Further improvement could be achieved by selective etching of the top GaAs contacting layer and deposition of an anti-reflection coating, thus greatly boosting the J_{sc}, in order to achieve current-matching with an underlying Si bottom cell.

ACKNOWLEDGEMENTS

This work is supported by Total SA.

REFERENCES

[1] Adachi S. GaAs, AlAs, and $Al_xGa_{1-x}As$: Material parameters for use in research and device applications. *J. Appl. Phys.* **58(**3) (1985) R1–R29, DOI: 10.1063/1.336070

[2] Vurgaftman I, Meyer JR, Ram-Mohan LR. Band parameters for III–V compound semiconductors and their alloys. *J. Appl. Phys.* **89**(11) (2001) 5815–5875, DOI: 10.1063/1.1368156

[3] Prior KA, Davies GJ, Heckingbottom R. The thermodynamics of oxygen incorporation into III-V semiconductor compounds and alloys in MBE. *J. Cryst. Growth* **66**(1) (1984) 55–62, DOI: 10.1016/0022-0248(84)90076-9

[4] Bhattacharya PK, Matsumoto T, Subramanian S. The relation of dominant deep levels in MOCVD $Al_xGa_{1-x}As$ with growth conditions. *J. Cryst. Growth* **68**(1) (1984) 301–304, DOI: 10.1016/0022-0248(84)90429-9

[5] Akimoto K, Kamada M, Taira K, Arai M, Watanabe N. Photoluminescence killer center in AlGaAs grown by molecular-beam epitaxy. *J. Appl. Phys.* **59**(8) (1986) 2833–2836, DOI: 10.1063/1.336938

[6] Amano C, Ando K, Yamaguchi M. The effect of oxygen on the properties of AlGaAs solar cells grown by molecular-beam epitaxy. *J. Appl. Phys.* **63**(8) (1988) 2853–2856, DOI: 10.1063/1.340938

[7] Islam MR, Chelakara RV, Neff JG, Fertitta KG, Grudowski PA, Holmes AL, Ciuba FJ, Dupuis RD, Fouquet JE. The growth and characterization of AlGaAs double heterostructures for the evaluation of reactor and source quality. *J. Electron. Mater.* **24**(6) (1995) 787–792, DOI: 10.1007/BF02659741

[8] Amano C, Shibukawa A, Yamaguchi M. $Al_{0.2}Ga_{0.8}As$ p^+-n junction solar cells grown by molecular beam epitaxy. *J. Appl. Phys.* **58**(7) (1985) 2780–2782, DOI: 10.1063/1.335871

[9] Amano C, Sugiura H, Ando K, Yamaguchi M, Saletes A. High-efficiency $Al_{0.3}Ga_{0.7}As$ solar cells grown by molecular beam epitaxy. *Appl. Phys. Lett.* **51**(14) (1987) 1075–1077, DOI: 10.1063/1.98744

[10] Melloch MR, Tobin SP, Bajgar C, Stellwag TB, Keshavarzi A, Lundstrom MS, Emery K. High-efficiency GaAs and AlGaAs solar cells grown by molecular beam epitaxy. *Proc. 21st IEEE PVSC* **1** (1990) 163–167, DOI: 10.1109/PVSC.1990.111611

[11] Yazawa Y, Kitatani T, Minemura J, Tamura K, Mochizuki K, Warabisako T. AlGaAs solar cells grown by MBE for high-efficiency tandem cells. *Sol. Energy Mater. Sol. Cells* **35** (1994) 39–44, DOI: 10.1016/0927-0248(94)90120-1

[12] Gale RP, Fan JCC, Turner GW, Chapman RL, Pantano JV. Efficient AlGaAs shallow-homojunction solar cells. *Appl. Phys. Lett.* **44**(6) (1984) 632–634, DOI: 10.1063/1.94859

[13] Virshup GF, Ford CW, Werthen JG. A 19% efficient AlGaAs solar cell with graded band gap. *Appl. Phys. Lett.* **47**(12) (1985) 1319–1321, DOI: 10.1063/1.96266

[14] Chung BC, Hamaker HC, Virshup GF, Werthen JG. 15% efficiency (1 sun, air mass 1.5), large-area, 1.93 eV $Al_xGa_{1-x}As$ (x=0.37) *n-p* solar cell grown by metalorganic vapor phase epitaxy. *Appl. Phys. Lett.* **52**(8) (1988) 631–633, DOI: 10.1063/1.99387

[15] Takahashi K, Minagawa Y, Yamada S, Unno T. Improved efficiency of $Al_{0.36}Ga_{0.64}As$ solar cells with a pp^-n^-n structure. *Sol. Energy Mater. Sol. Cells* **66**(1–4) (2001) 525–532, DOI: 10.1016/S0927-0248(00)00233-6

[16] Heckelmann S, Lackner D, Dimroth F, Bett AW. $Al_xGa_{1-x}As$ minority carrier lifetime enhancement at low temperatures. *Appl. Phys. Lett.* **103** (2013) 132102-1–132102-3, DOI: 10.1063/1.4822432

[17] Heckelmann S, Lackner D, Karcher C, Dimroth F, Bett AW. Investigations on $Al_xGa_{1-x}As$ Solar Cells Grown by MOVPE. *IEEE J. Photovolt.* **5**(1) (2015) 446–453, DOI: 10.1109/JPHOTOV.2014.2367869

[18] King RR, Bhusari D, Larrabee D, Liu XQ, Rehder E, Edmondson K, Cotal H, Jones RK, Ermer JH, Fetzer CM, Law DC, Karam NH. Solar cell generations over 40% efficiency. *Prog. in Photovol. Res. Appl.* **20**(6) (2012) 801–815, DOI: 10.1002/pip.1255

[19] Tang M, Wu J, Chen S, Jiang Q, Seeds AJ, Liu H, Dorogan VG, Benamara M, Mazur Y, Salamo G. Optimisation of the dislocation filter layers in 1.3-μm

InAs/GaAs quantum-dot lasers monolithically grown on Si substrates. *IET Optoelectron.* **9**(2) (2015) 61–64, DOI: 10.1049/iet-opt.2014.0078

[20] Chen S, Li W, Wu J, Jiang Q, Tang M, Shutts S, Elliott SN, Sobiesierski A, Seeds AJ, Ross I, Smowton PM, Liu H. Electrically pumped continuous-wave III–V quantum dot lasers on silicon. *Nat. Photonics* **10**(5) (2016) 307–311, DOI: 10.1038/nphoton.2016.21

[21] Onno A, Wu J, Jiang Q, Chen S, Tang M, Maidaniuk Y, Benamara M, Mazur YI, Salamo GJ, Harder NP, Oberbeck L, Liu H. 1.7eV $Al_{0.2}Ga_{0.8}As$ solar cells epitaxially grown on silicon by SSMBE using a superlattice and dislocation filters. *Proc. SPIE* **9743** (2016) 10-1–10-7, DOI: 10.1117/12.2208950

[22] Onno A, Wu J, Jiang Q, Chen S, Tang M, Maidaniuk Y, Benamara M, Mazur YI, Salamo GJ, Harder NP, Oberbeck L, Liu H. $Al_{0.2}Ga_{0.8}As$ solar cells monolithically grown on Si and GaAs by MBE for III-V/Si tandem dual-junction applications. *Energy Procedia* **92** (2016) 661–668, DOI: 10.1016/j.egypro.2016.07.037

[23] Cheng K-Y. Molecular beam epitaxy technology of III-V compound semiconductors for optoelectronic applications. *Proc. IEEE* **85**(11) (1997) 1694–1714, DOI: 10.1109/5.649646

[24] Roth T, Hohl-Ebinger J, Schmich E, Warta W, Glunz SW, Sinton RA. Improving the accuracy of Suns-V_{oc} measurements using spectral mismatch correction. *Proc. 33rd IEEE PVSC* **3** (2008) 1355–1359, DOI: 10.1109/PVSC.2008.4922686

[25] Richter M, Hammer MS, Sonnet T, Parisi J. Bandgap extraction from quantum efficiency spectra of $Cu(In,Ga)Se_2$ solar cells with varied grading profile and diffusion length. *Thin Solid Films* **633** (2017) 213–217, DOI: 10.1016/j.tsf.2016.08.022

[26] Morkoç H, Drummond TJ, Kopp W, Fischer R. Influence of Substrate Temperature on the Morphology of $Al_xGa_{1-x}As$ Grown by Molecular Beam Epitaxy. *J. Electrochem. Soc.* **129**(4) (1982) 824–826, DOI: 10.1149/1.2123980

[27] Alexandre F, Goldstein L, Leroux G, Joncour MC, Thibierge H, Rao EVK. Investigation of surface roughness of molecular beam epitaxy $Ga_{1-x}Al_xAs$ layers and its consequences on GaAs/$Ga_{1-x}Al_xAs$ heterostructures. *J. Vac. Sci. Technol. B* **3**(4) (1985) 950–955, DOI: 10.1116/1.583020

[28] Fischer R, Klem J, Drummond TJ, Thorne RE, Kopp W, Morkoç H, Cho AY. Incorporation rates of gallium and aluminum on GaAs during molecular beam epitaxy at high substrate temperatures. *J. Appl. Phys.* **54**(5) (1983) 2508–2510, DOI: 10.1063/1.332317